(27) Tanaka-Fukuda, T.; Omoto, M.; Inagaki, H. *Macromolecules* **1979**, *12*, 146.
(28) Richardson, M. J.; Savill, N. G. *Polymer* **1977**, *18*, 3.
(29) Wittmann, J. C.; Kovacs, A. J. *J. Polym. Sci., Part C* **1969**, *16*, 4443.
(30) Average values based on the data in: Brandrup, J.; Immergut, E. H., Eds. "Polymer Handbook"; Wiley: New York, 1975.
(31) Tanaka-Fukuda, T.; Omoto, M.; Inagaki, H. *Makromol. Chem.* **1981**, *182*, 2889.
(32) See, e.g.: Yamakawa, H. "Modern Theory of Polymer Solutions"; Harper and Row: New York, 1971.
(33) Stockmayer, W. H. *Makromol. Chem.* **1960**, *35*, 54.
(34) Because our systems are not perfectly symmetrical, this treatment is correct only in an approximate sense. At present, it is difficult to evaluate the error associated with this approximation, since there is no adequate theory of the second virial coefficient between chemically different polymers. However, it may be suggestive to note that according to the recent theory of Tanaka and Šolc,[35] the present approximation is adequate for a mixture of homologous polymers differing in molecular weight, insofar as the molecular weight difference does not exceed a factor of 1.5.
(35) Tanaka, G.; Šolc, K. *Macromolecules* **1982**, *15*, 791.
(36) (a) Kurata, M.; Fukatsu, H.; Sotobayashi, H.; Yamakawa, H. *J. Chem. Phys.* **1964**, *41*, 139. (b) Yamakawa, H. *Ibid.* **1968**, *48*, 2103.
(37) Yamakawa, H.; Tanaka, G. *J. Chem. Phys.* **1967**, *47*, 3991.
(38) Tanaka-Fukuda, T.; Inagaki, H. *Pure Appl. Chem.*, in press.
(39) Tanaka-Fukuda, T.; Nagata, M.; Inagaki, H., to be submitted to *Macromolecules*.

Combined Integrated and Dynamic Light Scattering by Poly(γ-benzyl glutamate) in a Helicogenic Solvent†

Manfred Schmidt

Institut für Makromolekulare Chemie, Universität Freiburg, Hermann-Staudinger-Haus, D-7800 Freiburg i.Br., West Germany. *Received August 1, 1983*

ABSTRACT: Simultaneous static and dynamic light scattering measurements were performed on poly(γ-benzyl glutamate) (PBG) in dimethylformamide (DMF) over a wide molecular weight range ($37\,000 \leq M_w \leq 560\,000$). The measurements independently demonstrate that the pitch of the helix formed by PBG in DMF is h = 1.5 Å, which coincides with the value found by Pauling and Corey for the α-helical structure in the solid state. The helix in solution cannot be described by a rigid rod but rather by a wormlike chain with considerable flexibility. By accounting in particular for the polydispersity of the samples the Kuhn statistical segment length was determined to be $\lambda^{-1} = 1400 \pm 100$ Å, which is smaller than reported in the literature. Theoretical calculations of the radius of gyration and of the hydrodynamic radius reveal that the neglect of polydispersity effects leads to an overestimate of the chain stiffness.

Introduction

Some time ago, Doty, Blout, and co-workers[1-4] found that under certain conditions, e.g., with slight variation of temperature or solvent composition, some polypeptides undergo a remarkably sharp transition from flexible or coiled structures to more or less rigid helices. Among these, PBG is one of the most thoroughly investigated polymers, and numerous publications deal with the cooperative phenomena of the helix–coil transition.[5-12] Others are concerned with the structure and the chain stiffness of the helix in solution.[13-23] The helix parameters have been explored for the solid state by means of X-ray diffraction[24,25] and still serve as helpful guides also for the helical structure in solution. However, it is still unclear whether the helical structure of PBG in solution is identical with the solid-state helix.

In solution long helical chains cannot be expected to show the behavior of completely rigid rods, but the helix will undergo bending motions which eventually will lead to a coiled structure in the limit of very large molecules. Commonly the chain stiffness is characterized by either the Kuhn preferential statistical length λ^{-1} or the Kratky–Porod persistence length a. In the Kuhn model[26] the segments of length λ^{-1} are considered as rigid rods linked together by flexible joints, whereas Kratky and Porod[27] considered a "limiting continuous chain",[28] which nowadays is commonly called the "wormlike" chain model. Kratky and Porod showed that in the limit of very long chains i.e., many Kuhn segments per chain, the Kuhn length is just twice the persistence length $\lambda^{-1} = 2a$. The persistence length is defined by the condition that the average scalar product of the two tangent vectors $\vec{b}_j$ and $\vec{b}_{j+n}$ at the chain positions j and $j + n$ has decayed to $1/e$, i.e., $\langle(\vec{b}_j\vec{b}_{j+n})\rangle = 1/e$, which corresponds to an average angle between the two ends of a persistence unit of $\vartheta = 68.4°$.

The purpose of the present paper is to demonstrate that a highly accurate determination of the persistence length is obtained if the measurements of static (or frequency integrated) (ILS) and of dynamic (or quasi-elastic) (QLS) light scattering are performed simultaneously.

Static light scattering has been frequently applied to study the rigidity of polymers in solution. Based on the Kratky–Porod wormlike chain model, the radius of gyration[29,30] and the particle scattering factor[31-33] were calculated for monodisperse and polydisperse systems. Unfortunately, uncertainties in the mass per unit length, M_L, and mostly unknown polydispersities of the samples made the interpretation of the static light scattering data somewhat ambiguous.

Theoretical investigations of flexible polymers suggested[34] that a combination of static and dynamic light scattering should allow a precise and extensive characterization of polymers in solution. The first simultaneously measured ILS and QLS results[35] confirmed these expectations, and it appeared natural to apply this combination of light scattering techniques also to stiff polymers. The main advantage of recording ILS and QLS simultaneously is the fact that the *same* set of photons is averaged (ILS) and correlated (QLS). Thus, the ILS and QLS data originate from the same source of scatterers.

Until recently,[36,37] there has been no adequate theoretical treatment of the influence of chain stiffness on QLS.

† This paper is dedicated to Prof. W. H. Stockmayer on the occasion of his 70th birthday, to whom I owe thanks for a wonderful time at Dartmouth College during the period 1980–1981.

0024-9297/84/2217-0553$01.50/0

Preliminary attempts have been undertaken by Fujime[38-40] and by Kubota and Chu,[41,42] who tried to interpret their QLS data on the basis of the free-draining model of Harris and Hearst (HH).[43] In general, the applicability of the HH model is restricted to rather low degrees of stiffness, since the normal coordinate approach cannot correctly describe a system, where the motion of the chain segments is strongly reduced, with a few degrees of freedom. Recently, it was estimated that for $\lambda L < 4$ the HH model yields reasonable results[37] if the nondraining approach of Hearst, Beals, and Harris (HBH)[44] is used instead of the free-draining approximation. For the present purpose we shall not use the HBH model because first, the HBH model employs the approximation of preaveraging the hydrodynamic interaction and second, because it seems difficult to include polydispersity effects.

Since the investigated PBG exhibit a nonnegligible molecular weight distribution, other model calculations for monodisperse systems were extended to polydisperse chains which obey a Schulz–Zimm[45,46] length distribution. These calculations do not differ from those published previously[37] and required some mostly numerical integrations. For details the reader is referred to the earlier paper.[37] Thus, only the theoretical results are given in the next section, which subsequently will be used for the interpretation of the combined ILS and QLS data.

Theory

ILS. An analytical expression is obtained for the radius of gyration for polydisperse, wormlike chains when a Schulz–Zimm-type distribution is assumed for the chain length. The weight distribution $W(L)$ is given by

$$W(L) = \frac{L^m}{m!} y^{m+1} \exp(-yL) \tag{1}$$

with $y = (m + 1)/L_w$ and L_w the weight-average contour length of the polymer. The experimentally obtained quantity is the z-average mean square radius of gyration, $\langle S^2 \rangle_z$, which in terms of the contour length L is defined as

$$\langle S^2 \rangle_z = \int_0^\infty W(L) L \langle S^2 \rangle \, dL / \int_0^\infty W(L) L \, dL \tag{2}$$

The radius of gyration of a monodisperse, wormlike chain was first calculated by Benoit and Doty[29]

$$\langle S^2 \rangle = \frac{L}{6\lambda} - \frac{1}{4\lambda^2} + \frac{1}{4L\lambda^3} - \frac{1}{8L^2\lambda^4}(1 - \exp(-2\lambda L)) \tag{3}$$

with λ^{-1} the Kuhn length. Substitution of eq 3 into (2) yields

$$\langle S^2 \rangle_z = \frac{m + 2}{6y\lambda} - \frac{1}{4\lambda^2} + \frac{y}{4(m + 1)\lambda^3} - \frac{1}{8m(m + 1)\lambda^4}\left(y^2 - \frac{y^{m+2}}{(y + 2\lambda)^m} \right) \tag{4}$$

The well-known limiting behavior for a Gaussian coil and for a rigid rod are recovered for $\lambda L \gg 1$ and $\lambda L \ll 1$, respectively.

$$\text{Gaussian coil:} \quad \langle S^2 \rangle_z = \frac{m + 2}{m + 1} \frac{L_w}{6\lambda} \tag{4a}$$

$$\text{rigid rod:} \quad \langle S^2 \rangle_z = \frac{(m + 3)(m + 2)}{(m + 1)^2} \frac{L_w^2}{12} \tag{4b}$$

QLS. In dynamic light scattering the intensity time correlation function (TCF) $G_2(t) = \langle i(0)i(t) \rangle$ is measured with $i(0)$ and $i(t)$, the scattering intensities at time $t = 0$ and $t = t$, respectively. For dilute solutions the electric field correlation function, $g_1(t)$, is obtained from the equation[47]

$$g_1(t) = \frac{\langle E(0)E^*(t) \rangle}{\langle E(0)E^*(0) \rangle} = \left[\frac{G_2(t) - A}{A} \right]^{1/2} \tag{5}$$

where A is the experimentally determined base line of the intensity TCF. $g_1(t)$ decays like a single exponential for narrow distributions of small scatterers and for monodisperse, rigidly spherical, optically isotropic particles of any size. In general, however, the TCF does not decay single exponentially, particularly, if the particle dimensions exceed $\lambda_s/20$, with λ_s the wavelength of the scattered light in the solution ($\lambda_s = \lambda_0/n$). In such cases, commonly a cumulant fit of the logarithmic TCF $g_1(t)$ is carried out[48] to describe the TCF at short delay times as

$$\ln (g_1(t)) = -\Gamma t + \mu_2(\Gamma t)^2/2 - \mu_3(\Gamma t)^3/6 + \ldots \tag{6}$$

$\Gamma = -[d \ln (g_1(t))/dt]_{t \to 0}$ is the first cumulant and μ_2 and μ_3 are dimensionless quantities which depend on the polydispersity and on the internal flexibility of the chain. For large particles the reduced first cumulant, Γ/q^2, depends on the scattering vector $q = (4\pi/\lambda_s) \sin(\theta/2)$, and can be written in the low-q limit as[36,49-51]

$$\Gamma/q^2 = D_z(1 + C\langle S^2 \rangle_z q^2 + \ldots) \tag{7}$$

In eq 7, D_z is the z-average translational diffusion coefficient and C a dimensionless quantity depending on the structure and polydispersity of the sample. C has been calculated for mono- and polydisperse linear and branched flexible polymers[34,49-51] and for monodisperse rigid rods[52,58] and wormlike chains.[36,37] According to Stokes and Einstein, a hydrodynamic radius (HR) can be obtained from the diffusion coefficient D_z

$$\langle 1/R_h \rangle_z^{-1} = kT/(6\pi\eta_0 D_z) \tag{8}$$

with kT the thermal energy and η_0 the solvent viscosity. The HR contains information on both the structure and the polydispersity, but in a different way from the radius of gyration. Thus the HR furnishes extra information to the radius of gyration. A few aspects of the HR and of C should be discussed to illustrate how in particular they could provide information about stiff polymers in solution.

Hydrodynamic Radius. The HR for polydisperse chains is given by

$$\langle 1/R_h \rangle_z^{-1} = \left[\int_0^\infty W(L) L R_h^{-1} \, dL / \int_0^\infty W(L) L \, dL \right]^{-1} \tag{9}$$

Inserting the flexible-coil limit for the HR according to Kirkwood[53]

$$R_h = b(6\pi)^{1/2} P^{1/2}/16 \tag{10}$$

with b the effective bond length and P the degree of polymerization, we obtain in the Gaussian limit

$$\langle 1/R_h \rangle_z^{-1} = 6^{1/2}(m + 1)!(2^{m+1} b P_w^{1/2}/[16(2(m + 1) - 1)!!(m + 1)^{1/2}]) \tag{11}$$

which leads for $m = 1$ to the well-known result

$$\langle 1/R_h \rangle_z^{-1} = bP_w^{1/2}/12^{1/2} \tag{11a}$$

Replacing R_h in eq 9 by its rigid rod limit due to Broersma[54]

$$R_h = L/(2(\ln (L/d) - \gamma)) \tag{12}$$

with γ a numerical constant and d the hydrodynamically effective diameter of the polymer, we obtain for polydisperse rigid rods

$$\langle 1/R_h \rangle_z^{-1} = \left[\frac{2y}{m+1} \left(\sum_{i=1}^{m} i^{-1} - C_E - \ln (yd) + \gamma \right) \right]^{-1} \quad (13)$$

with C_E the Euler constant and $y = (m + 1)/L_w$. Surprisingly, as long as the logarithmic term in eq 13 dominates, the HR for a rigid rod is virtually independent of polydispersity.

In recent years the HR for a Kratky–Porod chain was calculated by employing various approximations for the moments of the segment distribution function.[37,55,56] Here we follow the procedure given in ref 37, where Koyama's[33] expression for the segment distribution function was used, which yields

$$R_h = \left[\lambda(2/L^2) \int_0^L (L - s) B^{-1} \operatorname{erf}(B/2A)\, ds \right]^{-1} \quad (14)$$

with $A^2 = \langle R^2 \rangle (1 - \eta)/6$ and $B = \eta \langle R^2 \rangle$, where $2\eta^2 = 5 - 3\langle R^4 \rangle / \langle R^2 \rangle^2$. $\langle R^n \rangle$ denotes the nth moment of the Kratky–Porod distribution function. Inserting eq 14 into (9) we obtain a double integral, which has been solved numerically with the IMSL library program DCADRE.

Quantity C. For flexible structures the quantity C can be expressed in terms of the first three moments of the segment distribution[57]

$$C = \frac{1}{3} - \frac{\langle S \rangle}{5 \langle S^2 \rangle \langle S^{-1} \rangle} \quad (15)$$

with

$$\langle S^n \rangle = L^{-2} \int_0^L (L - s) \langle R(s)^n \rangle\, ds \quad (15a)$$

and

$$\langle R(s)^n \rangle = \int_0^\infty W(R,s) R^n (4\pi R^2)\, dR \quad (15b)$$

In eq 15, $W(R,s)$ represents the radial distribution function of the chain segments. For polydisperse systems

$$C = \frac{1}{3} - \frac{1}{5} \frac{\int_0^\infty W(L) L \langle S \rangle\, dL \int_0^\infty W(L) L\, dL}{\int_0^\infty W(L) L \langle S^2 \rangle\, dL \int_0^\infty W(L) L \langle S^{-1} \rangle\, dL} \quad (16)$$

Inserting into eq 16 the moments of the segment distribution for a Gaussian coil, we arrive at the result derived previously[50,51]

$$C = 1/3 - (2/25)(2 - (m + 2)^{-1}) \quad (17)$$

As discussed in ref 37, eq 15 cannot be applied to a rigid rod without removing the physical significance of the dynamic structure factor measured by QLS. Alternatively, it was proposed[37] that Pecora's formulation[58] of the dynamic structure factor of rigid rods be applied. Within this framework C was derived for the monodisperse case as[52]

$$C = (1/90)(L^2\Theta/D) \rightarrow 0.1 \quad \text{(thin rods)} \quad (18)$$

Here, Θ stands for the rotational diffusion coefficient. Taking into account the rotation–translation coupling for a rigid rod, Rallison and Leal[59] modified Pecora's expression for the dynamic structure factor. This results in a considerably lower value for C

$$C = \frac{\Theta L^2}{90D} - \frac{2\mu}{15} \rightarrow \frac{1}{30} \quad \text{(thin rods)} \quad (19)$$

where μ measures the anisotropy in translational diffusion, $\mu = 2(D_\parallel - D_\perp)/(D_\parallel + D_\perp)$. $D_\parallel$ and $D_\perp$ are the diffusion coefficients in directions parallel and perpendicular to the rod axis, respectively.

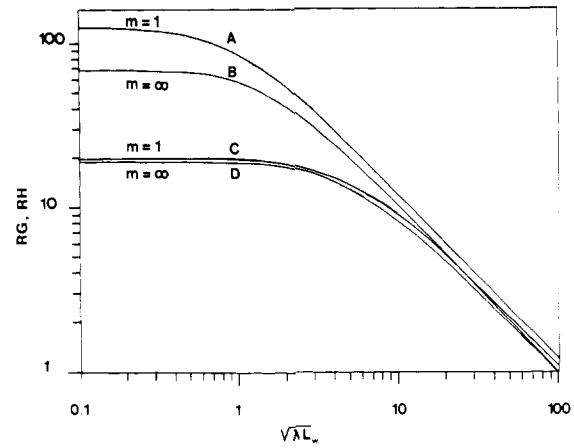

Figure 1. Calculated reduced quantities RG $\equiv \langle S^2 \rangle_z^{1/2} / \langle S^2 \rangle^{1/2}$(g,m) (g = Gaussian and m = monodisperse) (curves A and B) and RH $\equiv \langle 1/R_h \rangle_z^{-1} / R_h$(g,m) (curves C + D) plotted against $(\lambda L_w)^{1/2}$ for different polydispersities as attached to the curves. The ratio $L_w/d = 10^4$ is kept constant.

The slope C for polydisperse rigid rods is derived in the Appendix and is given by (the constants in D and Θ omitted)

$$C = \frac{1}{3} - \frac{7 + 4\mu}{30} \frac{m+1}{m+3} \frac{\sum_{i=1}^{m+2} i^{-1} - C_E - \ln (dy)}{\sum_{i=1}^{m} i^{-1} - C_E - \ln (dy)} \quad (20)$$

According to eq 20, C depends strongly on the polydispersity for the case of rigid rods. In the limiting cases $m = 1$ (Schulz–Flory distribution) and $m \rightarrow \infty$ (monodisperse), eq 20 yields $C = {}^{11}/_{60}$ and $C = {}^{1}/_{30}$, respectively, for infinitely thin rods.

Up to now we have not been able to derive a theoretical expression for the first cumulant of a wormlike chain which covers the whole region from a Gaussian coil to a rigid rod. In ref 37 it was suggested that the wormlike region be described by two approximations: (i) In the first approximation the moments $\langle S^n \rangle$ for a Kratky–Porod distribution function (in a form given by Koyama) are inserted into eq 15. This yields an approximate value for C which is correct in the Gaussian coil limit but becomes increasingly poor as the rigid rod limit is approached. It is believed that this procedure yields suitable results for $\lambda L > 4$–10. (ii) In the other approximation eq 19 for a rigid rod is assumed to be essentially correct also for a weakly bending rod. This approach neglects the influence of bending modes (which indeed are most likely not observable on the experimental time scale of the present QLS instruments, at least not in the very stiff limit) but takes into account the change in the rotational diffusion coefficient with increasing chain flexibility suggested by the Monte Carlo study by Hagerman and Zimm.[60] These results are meaningful for $\lambda L \leq 2.5$. For monodisperse wormlike chains a rather reliable interpolation between the approximations i and ii could be obtained.[37] Subsequent numerical integration over the Schulz–Zimm chain length distribution is easily performed, and the results are shown in Figures 1–3 together with the other relevant quantities concerning the hydrodynamic radius and the radius of gyration.

Figure 1 shows the effect of polydispersity and of chain stiffness on the radius of gyration and on the HR, respectively. For convenience, reduced quantities i.e., normalized by their monodisperse, Gaussian values, are

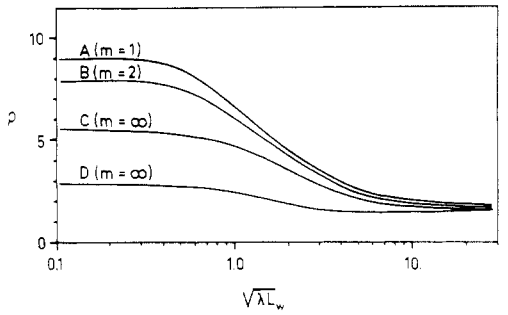

Figure 2. Calculated ratio $\rho \equiv \langle S^2\rangle_z^{1/2}\langle 1/R_h\rangle_z$ for different polydispersities as a function of $(\lambda L_w)^{1/2}$. Curves A–C, $L_w/d = 10^4$; curve D, $L_w/d = 10^{12}$.

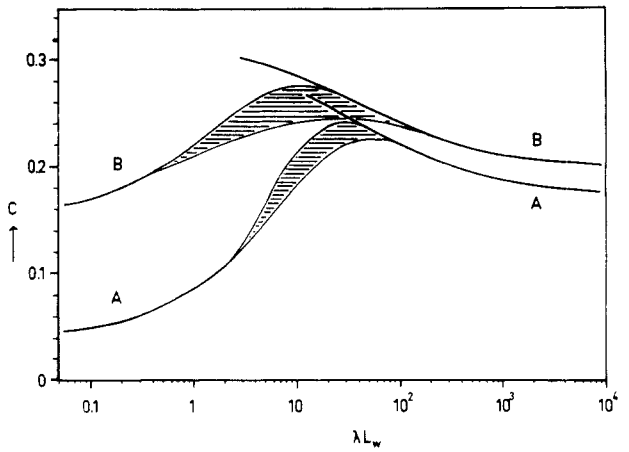

Figure 3. Calculated dimensionless quantity C plotted against λL_w for $L_w/d = 10^6$. Curve A shows a monodisperse ($m = \infty$) and curve B a Schulz–Flory ($m = 1$) distribution. The full curves are calculated by employing the approximations for the stiff and the flexible limits, respectively, as described in the text. The shaded area represents the author's estimate for an interpolation between the two approaches.

plotted against the square root of the reduced length λL on a double-logarithmic scale. The influence of polydispersity on the radius of gyration (curves A and B) is larger than on the HR (curves C and D). The magnitude of the latter effect (i.e., at most 6.4% in the flexible limit) is almost within the experimental error of current light scattering instruments. The sensitivity of the radius of gyration to polydispersity increases as the chain stiffness increases. For polymers smaller than 30 Kuhn lengths the HR is only slightly affected by increasing the persistence length, keeping the contour length of the molecule constant.

The ratio ρ of both quantities, $\rho = \langle S^2\rangle_z^{1/2}/\langle 1/R_h\rangle_z^{-1}$ shows qualitatively the same behavior. Curves C and D in Figure 2 demonstrate the effect of the hydrodynamically effective cross section d of a polymer, which changes the HR and accordingly ρ remarkably. In contrast to flexible chains, where the chain cross section has only little effect on the hydrodynamic behavior, it is particularly this cross section, or more precisely the geometric anisotropy, which increasingly governs the hydrodynamic behavior when the structure becomes more rigid.

The dimensionless quantity C is plotted in Figure 3 for monodisperse (curve A) and for polydisperse (curve B) structures. The full curves correspond to the two approximations near the Gaussian limit and near the rod limit, as mentioned earlier. The shaded area represents the author's estimate for a reasonable interpolation between the two approaches. This estimate becomes increasingly indefinite as the polydispersity increases. However, the existence of a maximum is evident, the height of which becomes more pronounced as the ratio L_w/d increases. Unfortunately, neither the position nor the height of this maximum is exactly known.

This theoretical outline demonstrates that each of the introduced four quantities ($\langle S^2\rangle_z$, $\langle 1/R_h\rangle_z^{-1}$, ρ, and C) depends both on the polydispersity and on the chain stiffness. The exact knowledge of these parameters characterizes a polymer structure fairly comprehensively.

Experimental Section

The PBG samples were prepared at the chemical laboratory of the CNRS, Strasbourg, according to standard procedures[61] and were kindly provided by Dr. E. Marchal. The unfractionated samples exhibited a molecular weight distribution, usually with polydispersities of $1.6 \leq M_w/M_n \leq 2$. The highest molecular weight, however, had a broader distribution ($M_w/M_n \approx 3$). The number-average molecular weight, M_n, was determined by membrane osmometry and the weight-average molecular weight, M_w, by light scattering. These polydispersities agree qualitatively with earlier estimates based on dielectric dispersion measurements.[23]

Osmometry. Osmotic pressure measurements were performed with a Hewlett-Packard membrane osmometer HP 505 in DMF at 30 °C. Regenerated cellulose membranes were used (Type P400, Fa. Kalle, Wiesbaden). The reduced osmotic pressure π/c was extrapolated to zero concentration. For this, four different concentrations ranging from 3 to 15 mg/mL were employed.

Light Scattering. ILS and QLS measurements were performed with a Malvern K7023 96-channel correlator connected to a light scattering spectrometer,[35] which allows the simultaneous recording of the scattering intensity and of the correlation function. A krypton ion laser (Spectra Physics, Model Kr 164-11) was used as light source operating at 647.1-nm wavelength.

For the light scattering measurements PBG was dissolved in dried and freshly distilled DMF at least 48 h prior to measurement. The concentration ranged from 3 to 15 mg/mL for the smallest molecular weight down to 0.6 to 7 mg/mL for the highest molecular weight. All samples were clarified by using a Beckman ultracentrifuge L50 with a swinging bucket rotor (Model SW 25.1), applying a special floating technique[62] with cesium chloride as the density agent. The centrifugation time was varied from 1 to 2.5 h at 15000 rpm (=22000g), depending on the molecular weight.

Data Analysis. As mentioned earlier the TCF was analyzed according to the method of cumulants (eq 6). In most cases a two-cumulant fit described the data satisfactorily and a third cumulant did usually not improve the variance significantly. For the lower molecular weights ($M_w < 10^5$) a sample time τ was selected which fulfilled the condition $\Gamma t_{max} = \Gamma\tau n_{max} \approx 5$, with n_{max} the last channel in the correlator. Although our correlator is equipped with 96 channels only, for the present measurements n_{max} equals 348, because a delay of 256τ occurs after the first 80 channels (four channels are lost for this delay); the last 12 channels from 337τ to 348τ are used to monitor the base line. For long enough sample times the measured and the statistically calculated base line coincided better than 1‰. Reduction of the sample time by a factor of 2 did not cause a significant change of the first cumulant, i.e., within the experimental error of 2 or 3%. This was no longer true for the three highest molecular weight samples. Upon reduction of the sample time the first cumulant increased significantly. In addition, a very slow relaxation process (much slower than the translational diffusion) became detectable. This long relaxation time is not caused by dust or other artifacts and could not be neglected. Analysis of the full TCF in terms of a relaxation time distribution using numerical Laplace inversion is in progress with the CONTIN program by Provencher.[63,64] The results will be published separately elsewhere. The present paper is confined solely to the evaluation of the first cumulant, which contains contributions of the translational diffusion coefficient and of the internal modes of motion. To this end, measurements were made with decreasing sample times until the first cumulant did not change on further reduction of the sample time. Usually for $\Gamma t_{max} \leq 0.5$ the first cumulant remained constant, and these data were taken for the interpretation of the chain stiffness. (For the shortest sample times the TCF did not reach the base line, in spite of the 256-channel delay. Then we always normalized $G_2(t)$ by the statistically measured base line, i.e., employing the

Table I
Experimental Results for PBG in DMF

$M_w \times 10^{-3}$, dalton	$M_n \times 10^{-3}$, dalton	R_h,[a] Å	$\langle S^2 \rangle_z^{1/2}$, Å	A_2, (cm³ mol)/g²	k_d, cm³/g	k_{f_0},[b]	c
38	29	46		3.7	2.0	1.2	
73	43	77	183	3.3	6.8	1.4	
80	48	82	197	3.0	3.9	1.8	
95	55	97	240	2.5	4.9	1.8	
200	101	167	483	3.1	15.0	2.5	
210	128	175	500	2.5	18.6	2.7	0.15
560	190	360	1010	2.5	33.5	4.4	0.19

[a] $R_h \equiv \langle 1/R_h \rangle_z^{-1} = kT/(6\pi\eta_0 D_z)$. [b] As defined by eq 25.

monitor channels.) Such a fitting procedure appears somewhat artificial and actually needs theoretical justification. At the present time it can be argued qualitatively, only, that as the time scale (i.e., the sample time) of the correlator is reduced, faster processes (i.e., relaxation times) can be detected, which surely exist in a wormlike chain. This suggests that for the present system "bending modes" become observable for molecules larger than one Kuhn length λ^{-1}. Accordingly, the theoretical "rigid rod" approach to the slope C (which only accounts for rotational diffusion) underestimates C, as will be discussed later (see Figure 6). Moreover, a time-dependent slope $C(t)$ should be observed,[65] which at very small times reaches the limit of the zero time slope C calculated in the theoretical section for the "unconstrained" approximation. Unfortunately, as the sample time is reduced, the noise in the TCF increases significantly and a cumulant fit becomes increasingly inaccurate. Further investigation of this problem is in progress.

The ILS data were plotted in Zimm plots, which allow the evaluation of the weight-average molecular weight, M_w, of the z-average mean square radius of gyration, $\langle S^2 \rangle_z$, and of the second virial coefficient A_2, as usual. A similar "dynamic" Zimm plot was suggested[35] for the reduced first cumulant where Γ/q^2 replaces the reduced scattering intensity Kc/R_θ in the "static" Zimm plot. One example for Zimm plots of simultaneously measured ILS and QLS data is given in Figure 4. The "dynamic" Zimm plot yields the infinite-dilution value of D_z as the concentration and the magnitude of the scattering vector, q, approaches zero. This procedure is analogous to the determination of the molecular weight in the static Zimm plot. The slope against q^2 extrapolated to zero concentration yields $C\langle S^2 \rangle_z$, with C the structure-dependent, dimensionless quantity discussed in the theoretical section. The slope against c for $q \to 0$ gives $k_d D_z$, where k_d describes the concentration dependence of the translational diffusion coefficient according to

$$D_z(c) = D_z(0)(1 + k_d c) \qquad (21)$$

Results and Discussion

The measured data of all PBG's are listed in Table I. In Figure 5 the radius of gyration and the HR are plotted against the molecular weight M_w on a double-logarithmic scale. The data fall on a slightly bent curve and cannot be described by simple power laws. We fitted therefore the data according to eq 4 and 9 given in the theoretical section. As mentioned in the Introduction, uncertainties in the length per monomeric residue, h, make the analysis of the radius of gyration somewhat ambiguous, since slight variation in h can easily be compensated by a change of the Kuhn length λ^{-1} or of the polydispersity of the samples. This is no longer true for the HR, which, at least in the λL region investigated here, depends essentially on the contour length $L_w = hP_w$ (P_w is the degree of polymerization) and on the hydrodynamically effective cross section of the polymer. The HR changes only slightly with polydispersity and hardly at all with chain stiffness. A good fit to the hydrodynamic data was achieved with $h = 1.5$ Å, precisely the value found by Pauling and Corey[24,25] for the α-helix, and with the diameter of the helix $d = 30$ Å. The latter value appears a little high and it seems possible to reduce d by increasing h. Indeed, reducing d to 25 Å and increasing h to 1.6 Å yield a similar curve with a slightly different curvature. Smaller values than $h = 1.5$ Å cannot fit the data satisfactorily, irrespectively of the

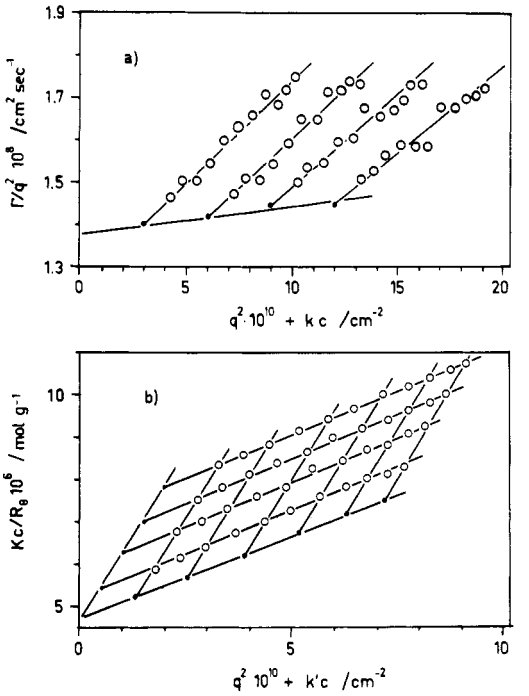

Figure 4. "Dynamic" (a) and "static" (b) Zimm plots for the sample of $M_w = 210\,000$. For the dynamic Zimm plot the usual zero-concentration extrapolation of the data at finite scattering angles could not be performed because the data scatter too much due to the extended scale of Γ/q^2.

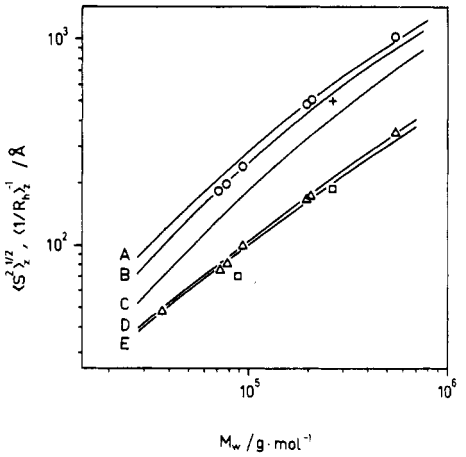

Figure 5. Experimental data and theoretical curves for the radius of gyration, $\langle S^2 \rangle_z^{1/2}$ (upper data, curves A–C) and for the hydrodynamic radius, $\langle 1/R_h \rangle_z^{-1}$ (lower data, curves D and E) plotted against the molecular weight, M_w. (○) $\langle S^2 \rangle_z^{1/2}$, this work; (+) $\langle S^2 \rangle_z^{1/2}$ from ref 42; (△) $\langle 1/R_h \rangle_z^{-1}$, this work; (□) $\langle 1/R_h \rangle_z^{-1}$ from ref 42. The theoretical curves represent different polydispersities: curves A and D, $m = 1$; curves B and E, $m = 2$; curve C, $m = \infty$.

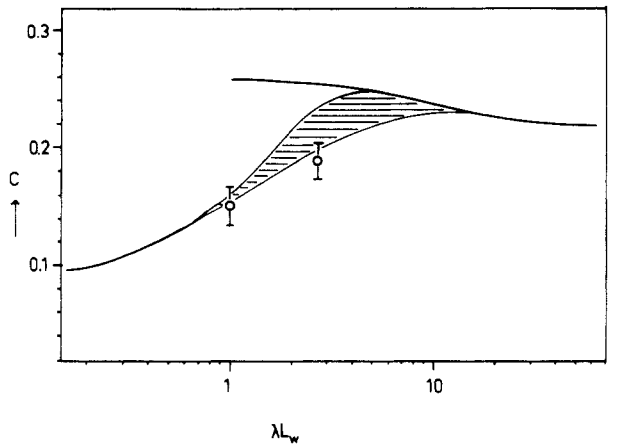

Figure 6. Experimental data for the quantity C are plotted against λL_w. For comparison the calculated quantity C is given using $m = 1$, $d = 30$ Å, and $\lambda^{-1} = 1400$ Å. Full curves and the shaded area are described in Figure 3.

value for d. We now obtain the Kuhn length and a good approximation for the polydispersity from the fit of the radius of gyration by eq 4. This is shown in Figure 5 for $h = 1.5$ Å, where three theoretical curves are plotted for the radius of gyration for the monodisperse case (curve C), for a Schulz–Zimm distribution ($m = 2$, $M_w/M_n = 1.5$, curve B), and for a Schulz–Flory distribution ($m = 1$, $M_w/M_n = 2$, curve A). The Kuhn length is $\lambda^{-1} = 1400$ Å. It is clearly seen that the highest molecular weight samples are well described by the theoretical curve A, whereas the small molecular weights are better fitted by curve B. This behavior is in qualitative agreement with the polydispersities given in Table I. The value of $\lambda^{-1} = 1400$ Å found from the analysis appears to be too small compared to literature values of $\lambda^{-1} = 1700$–2800 Å. Although λ^{-1} could still vary by ±100 Å within experimental error, this cannot explain the difference from the literature values. It follows from curve C in Figure 5 for monodisperse samples that the neglect of polydispersity effects would lead to a serious overestimate of the chain stiffness. Of course, the radius of gyration can be fitted to the data by employing a larger value for the pitch of the helix of $h = 1.6$ Å. This results in an even smaller Kuhn length of $\lambda^{-1} = 1200$ Å.

Recently, Kubota and Chu[42] published ILS and QLS data for two PGB samples also measured in DMF but at a slightly higher temperature (25 °C). For comparison these data are included in Figure 5. The radius of gyration of the higher molecular weight sample is significantly smaller as compared to the present measurements. The HR, however, lies, within experimental error, on the same curve as our values, thus supporting our method of data evaluation. Again, this can be explained by a smaller polydispersity of the sample measured by Kubota and Chu. Indeed, a fit of the radius of gyration according to eq 4 is possible, if $M_w/M_n = 1.33$ (corresponding to $m = 3$) is assumed, which is very close to the value of $M_w/M_n = 1.26$ evaluated by Kubota and Chu. The HR of the smaller molecular weight sample deviates strongly from our measurements. However, since only approximate values were reported for this sample, the discrepancy is not serious.

As discussed in the theoretical part the angular dependence of the reduced first cumulant contains additional information about the chain stiffness. The quantity C can be measured if $u^2 = q^2\langle S^2\rangle_z > 1$. For the investigated PBG samples this condition is fulfilled for the three highest molecular weight samples only. Two examples for the determination of C are shown in Figures 7 and 8. In Figure 7, $\Gamma/q^2D_{z,c}$ is plotted against $u_c = q^2\langle S^2\rangle_{z,c}$, where

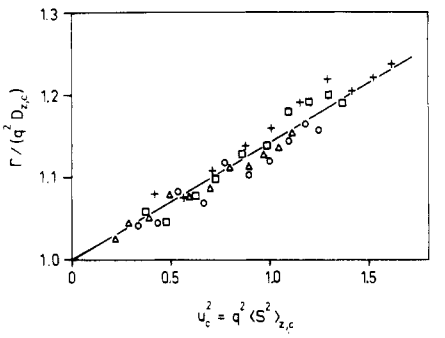

Figure 7. Reduced first cumulant $\Gamma/(q^2D_z)$ plotted against $u_c^2 = q^2\langle S^2\rangle_{z,c}$ for the sample of $M_w = 210\,000$ at four concentrations: (+) c_0; (□) $3c_0/4$, (○) $c_0/2$; (△) $c_0/4$ ($c_0 = 5.88$ mg/mL). The slope is equal to C.

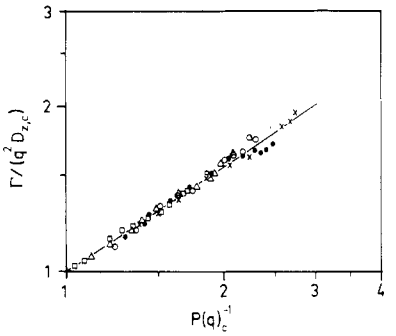

Figure 8. Reduced first cumulant $\Gamma/(q^2D_{z,c})$ vs. the inverse particle scattering factor, $P(q)_c^{-1}$, for the sample of $M_w = 560\,000$ at five concentrations: (×) c_0; (●) $c_0/2$; (○) $3c_0/10$; (△) $c_0/5$; (□) $c_0/10$ (c_0 6.34 mg/mL). The slope equals $3C$.

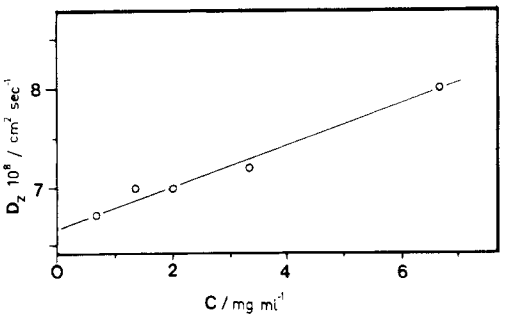

Figure 9. Translational diffusion coefficient, D_z, plotted against the concentration c for the sample of $M_w = 560\,000$. The slope yields $k_d = 33.5$ cm³/g.

the index c marks the data measured at finite concentration c. Within experimental error no concentration dependence of C was detectable. Especially for large polymers it has been suggested[34] that C be determined from a double-logarithmic plot of $\Gamma/q^2D_{z,c}$ against the inverse particle scattering factor $1/P(q)_c$. Such a plot should exhibit an extended linear region, the slope of which equals $3C$. Figure 8 shows the plot for the sample of $M_w = 560\,000$. Again, no concentration dependence of C is observed.

Of course, two experimental values of C are not sufficient to make any interpretation in terms of chain stiffness. As shown in Figure 6 both values of C lie slightly below the theoretical estimates. The deviation might be due to the fact that within the experimental time scale of the correlator the zero-time value of C is not yet reached. This point needs further theoretical and experimental investigation.

Figure 9 shows the concentration dependence of the translational diffusion coefficient D_z for the sample of $M_w = 560\,000$. The absolute linearity of the data suggests that

the measured concentrations are below the overlap concentration c^*, which may be defined for a wormlike chain via the hydrodynamic volume V_h

$$c^* = M_w/(V_h N_A) \tag{22}$$

with N_A the Avogadro number and

$$V_h = (4\pi/3)R_h^3 \tag{23}$$

The slope, k_d, of D_z against c contains information about the solvent quality and is directly related to the second virial coefficient, A_2, and to the concentration dependence, k_f, of the friction coefficient (i.e., $f(c) = f(0)(1 + k_f c)$) according to

$$k_f + k_d = 2A_2M + \nu_2 \tag{24}$$

with ν_2 the partial specific volume of the polymer. k_f may be expressed as[66-68]

$$k_f = k_{f0}N_A V_h/M \tag{25}$$

with V_h as defined in eq 23. k_{f0} is the interpenetration parameter which has been calculated by various authors for soft and hard spheres simulating a Θ and a good solvent for Gaussian coils, respectively. The k_{f0} values were evaluated according to eq 23–25 by employing the experimentally determined data for M_w, A_2, and R_h. The low molecular weight samples exhibit a k_{f0} value which lies below the theoretical soft-sphere value of 2.23.[68] With increasing chain length k_{f0} increases to 4.4. This value ought to be compared to the theoretical calculation for a hard sphere of $k_{f0} = 7.14$.[68] Since k_{f0} has not yet been calculated for rigid rods or wormlike chains, the presented experimental values are given without further comment.

Summary and Conclusion

Combined ILS and QLS measurements are demonstrated to be a powerful technique for the characterization of stiff polymers in solution. The analysis of the molecular weight dependence of the HR and of the radius of gyration allowed the molecular parameters of the helix to vary within experimental error between $h = 1.5$ Å, $d = 30$ Å, and $\lambda^{-1} = 1400$ Å and $h = 1.6$ Å, $d = 25$ Å, and $\lambda^{-1} = 1200$ Å, respectively. We tend to favor the first set of parameters because, first, the hydrodynamically effective cross section, d, of polymers in solution is expected to be larger than the geometric diameter in the solid state. This originates from the fact that solvent molecules stick to the helix surface, thus contributing to the friction of the polymer. Second, the determined Kuhn length $\lambda^{-1} = 1400$ Å is already much smaller than reported in the literature so that $\lambda^{-1} = 1200$ Å appears to be too low. However, theoretical calculations of the HR and of the radius of gyration reveal that the neglect of polydispersity effects leads to a serious overestimate of the chain stiffness.

The angular dependence of the reduced first cumulant Γ/q^2 or the slope C could be calculated approximately only. The experimentally determined values for C are smaller than the theoretical estimates. The deviation is explained by the limited time resolution of current correlators, which do not measure the zero-time value $C(t = 0) \equiv C$ but rather a quantity $C(t)$, which approaches zero as $t \to \infty$. At present it seems highly improbable that the angular dependence of Γ/q^2 can be utilized to determine chain stiffness. It rather appears that further theoretical and experimental effort is needed for the understanding of the dynamic behavior of wormlike chains in solution.

Acknowledgment. We are indebted to Prof. W. Burchard, Freiburg, for fruitful discussions and valuable suggestions. The PBG samples were kindly provided by Dr. E. Marchal, Strasbourg, who is gratefully acknowledged. We thank Dr. S. B. Ross-Murphy for reading and correcting the manuscript. The osmotic pressure measurements were kindly performed by Mr. F. Herzog. This work was supported by the Deutsche Forschungsgemeinschaft with a personal stipend.

Appendix

The dynamic structure factor $S(q,t)$ for rigid rods including translation–rotation coupling is given by[37,59]

$$S(q,t) = \exp(-q^2Dt) \times \{a_0 \exp(+q^4\mu^2D^2t/30\Theta) + a_2 \exp(-6\Theta t) \exp(-2q^2\mu Dt/7)\} \tag{A1}$$

$$a_0 = 1 - q^2L^2/36 + q^4L^4/32400 \tag{A1a}$$

$$a_2 = q^4L^4/6480 - q^4L^2\mu D/540\Theta + q^4\mu^2D^2/180\Theta^2 \tag{A1b}$$

For polydisperse systems the integral $\int_0^\infty W(L)LS(q,t)\,dL$ has to be evaluated; $W(L)$ is defined by eq 1 in the main text. The reduced first cumulant, Γ/q^2, is then calculated as

$$\Gamma/q^2 = \left[\int_0^\infty W(L)L\,dL\{a_0(D - q^2\mu^2D^2/30\Theta) + a_2(D + 6\Theta/q^2 + 2\mu D/7)\}\right] \Big/ \left[\int_0^\infty W(L)L(a_0 + a_2)\,dL\right] \tag{A2}$$

Inserting Broersma's expression for D and Θ, one can easily evaluate the integrals involved in eq A2. Neglecting all $\mathcal{O}(q^4)$, one can eventually generate the coefficient C of the q^2 term given in the main text.

Registry No. Poly(γ-benzyl glutamate) (homopolymer), 25014-27-1; poly(γ-benzyl glutamate) (SRU), 25038-53-3.

References and Notes

(1) Doty, P.; Holtzer, A. M.; Bradbury, J. H.; Blout, E. R. *J. Am. Chem. Soc.* **1954**, *76*, 4493.
(2) Doty, P.; Yang, J. T. *J. Am. Chem. Soc.* **1956**, *78*, 498.
(3) Doty, P.; Bradbury, J. H.; Holtzer, A. M. *J. Am. Chem. Soc.* **1956**, *78*, 947.
(4) Doty, P.; Lundberg, R. D. *J. Am. Chem. Soc.* **1956**, *78*, 4810.
(5) Ford, N. C.; Lee, W.; Karasz, F. E. *J. Chem. Phys.* **1969**, *50*, 3099.
(6) Dufour, C.; Marchal, E. *Biopolymers* **1972**, *11*, 1, 21.
(7) Strazielle, C.; Dufour, C.; Marchal, E. *Eur. Polym. J.* **1970**, *6*, 1133.
(8) Marchal, E.; Dufour, C.; Strazielle, C. *Eur. Polym. J.* **1970**, *6*, 1147.
(9) Tsvetkov, V. N.; Shtennikova, I. N.; Ryumtsev, Ye. I.; Pirogova, G. F. *Polym. Sci. USSR (Engl. Transl.)* **1967**, *9*, 1780.
(10) Takashima, S. *Biopolymers* **1963**, *1*, 171.
(11) Takashima, S. *Biopolymers* **1966**, *4*, 633.
(12) Watanabe, H.; Yoshioka, K.; Wada, A. *Biopolymers* **1961**, *2*, 91.
(13) Spach, G.; Freund, L.; Daune, M.; Benoit, H. *J. Mol. Biol.* **1963**, *7*, 468.
(14) Fujita, A.; Teramoto, A.; Yamashita, T.; Okita, K.; Ikeda, S. *Biopolymers* **1966**, *4*, 781.
(15) Fujita, H.; Teramoto, A.; Okita, K.; Yamashita, T.; Ikeda, S. *Biopolymers* **1966**, *4*, 769.
(16) Moha, P.; Weill, G.; Benoit, H. *J. Chem. Phys.* **1964**, *61*, 1239.
(17) Nishinari, K.; Yoshioka, K. *Kolloid Z. Z. Polym.* **1970**, *240*, 831.
(18) Ohe, H.; Watanabe, H.; Yoshioka, K. *Kolloid Z. Z. Polym.* **1973**, *252*, 26.
(19) Watanabe, H.; Yoshioka, K.; Lada, A. *Biopolymers* **1964**, *2*, 91.
(20) Wada, A. *J. Chem. Phys.* **1959**, *30*, 328.
(21) Wada, A. *J. Chem. Phys.* **1959**, *31*, 495.
(22) Marchal, E.; Marchal, J. *J. Polym. Sci., Part C* **1968**, *16*, 4019.
(23) Marchal, E.; Marchal, J. *J. Chim. Phys. Phys.-Chim. Biol.* **1967**, *64*, 1607.
(24) Pauling, L.; Corey, R. B.; Branson, H. R. *Proc. Natl. Acad. Sci. U.S.A.* **1951**, *37*, 205.
(25) Pauling, L.; Corey, R. B. *Proc. Natl. Acad. Sci. U.S.A.* **1959**, *81*, 3902.
(26) Kuhn, W. *Kolloid Z.* **1934**, *68*, 2.
(27) Kratky, O.; Porod, G. *Recl. Trav. Chim. Pays-Bas* **1949**, *68*, 1106.
(28) Daniels, H. E. *Proc.—R. Soc. Edinburgh, Sect. A: Math., Phys. Sci.* **1952**, *63*, 290.
(29) Benoit, H.; Doty, P. *J. Phys. Chem.* **1953**, *57*, 958.

(30) Burchard, W. *Br. Polym. J.* **1971**, *3*, 209.
(31) Franken, I.; Burchard, W. *Macromolecules* **1973**, *6*, 848.
(32) Yamakawa, H.; Fujii, M. *Macromolecules* **1974**, *7*, 649.
(33) Koyama, R. *J. Phys. Soc. Jpn.* **1973**, *34*, 1029.
(34) Burchard, W.; Schmidt, M.; Stockmayer, W. H. *Macromolecules* **1980**, *13*, 1265.
(35) Bantle, S.; Schmidt, M.; Burchard, W. *Macromolecules* **1982**, *15*, 1604.
(36) Stockmayer, W. H.; Schmidt, M. *Pure Appl. Chem.* **1982**, *54*, 407.
(37) Schmidt, M.; Stockmayer, W. H., in preparation.
(38) Fujime, S. *J. Phys. Soc. Jpn.* **1970**, *29*, 752.
(39) Fujime, S.; Maruyama, M. *Macromolecules* **1973**, *6*, 237.
(40) Maeda, T.; Fujime, S. *Macromolecules* **1981**, *14*, 809.
(41) Kubota, K.; Chu, B. *Macromolecules* **1983**, *16*, 105.
(42) Kubota, K.; Chu, B. *Biopolymers* **1983**, *22*, 1461.
(43) Harris, R. A.; Hearst, J. E. *J. Chem. Phys.* **1966**, *44*, 2595.
(44) Hearst, J. E.; Beals, E.; Harris, R. A. *J. Chem. Phys.* **1968**, *48*, 537.
(45) Schulz, G. V. *Z. Phys. Chem. (Leipzig)* **1939**, *43*, 25.
(46) Zimm, B. H. *J. Chem. Phys.* **1948**, *16*, 1099.
(47) Siegert, A. J. F. *MIT Rad. Lab.* **1943**, *Rep. No. 465*.
(48) Koppel, D. E. *J. Chem. Phys.* **1972**, *57*, 4814.
(49) Burchard, W. *Macromolecules* **1978**, *11*, 455.
(50) Schmidt, M.; Burchard, W. *Macromolecules* **1978**, *11*, 460.
(51) Burchard, W.; Schmidt, M.; Stockmayer, W. H. *Macromolecules* **1980**, *13*, 580.
(52) Mueller, M.; Burchard, W. *Int. J. Biol. Macromol.* **1981**, *3*, 71.
(53) Kirkwood, J. G.; Riseman, J. *J. Chem. Phys.* **1948**, *16*, 565.
(54) Broersma, S. *J. Chem. Phys.* **1960**, *32*, 1626.
(55) Yamakawa, H.; Fujii, M. *Macromolecules* **1973**, *6*, 407.
(56) Hearst, J. E.; Stockmayer, W. H. *J. Chem. Phys.* **1967**, *47*, 1396.
(57) Tanaka, G.; Stockmayer, W. H. *Proc. Natl. Acad. Sci. U.S.A.* **1982**, *79*, 6401.
(58) Berne, B.; Pecora, R. "Dynamic Light Scattering"; Wiley: New York, 1976.
(59) Rallison, J. M.; Leal, L. G. *J. Chem. Phys.* **1981**, *74*, 4819.
(60) Hagerman, P.; Zimm, B. H. *Biopolymers* **1981**, *20*, 1481.
(61) Marchal, E. *J. Chim. Phys.* **1966**, *63*, 1247.
(62) Dandliker, W. B.; Kraut, J. *J. Am. Chem. Soc.* **1956**, *78*, 2380.
(63) Provencher, S. W. *Comput. Phys. Commun.* **1982**, *27*, 213.
(64) Provencher, S. W. *Comput. Phys. Commun.* **1982**, *27*, 229.
(65) Schmidt, M.; Stockmayer, W. H.; Mansfield, M. *Macromolecules* **1982**, *15*, 1609.
(66) Imai, S. *J. Chem. Phys.* **1969**, *50*, 2116.
(67) Yamakawa, H. *J. Chem. Phys.* **1962**, *36*, 2995.
(68) Pyun, C. W.; Fixman, M. *J. Chem. Phys.* **1964**, *41*, 937.

Rotational Motion of the Ester Methyl Group in Stereoregular Poly(methyl methacrylate): A Neutron Scattering Study

Barbara Gabryś,* Julia S. Higgins, Karen T. Ma, and Jaan E. Roots

Department of Chemical Engineering and Chemical Technology, Imperial College, London SW7 2BY, England. *Received August 2, 1983*

ABSTRACT: Quasi-elastic neutron scattering data are reported for two stereoisomers of poly(methyl methacrylate) in which all but the ester methyl hydrogens have been replaced with deuterium. For syndio- and isotactic forms the observed motion is dominantly a threefold symmetric rotation about the O–CH_3 bond but the behavior in both cases is non-Arrhenius, with an apparent activation energy reducing from 7 kJ mol^{-1} above room temperature to 1 kJ mol^{-1} at 150 K. This behavior is explained by the inclusion of higher terms in the Fourier series expansion of the potential function for the methyl group rotation. Differences observed at lower temperatures in the absolute magnitude of the rotational rates for the stereoisomers are explained in terms of the relative angular phase of the threefold and higher Fourier terms in the potential.

1. Introduction

The intramolecular motion in polymers is manifested, for instance, in their dynamical-mechanical behavior.[1] Large-scale conformational rearrangements arising from rotations about backbone bonds are frozen in at the glass transition temperature, but even at lower temperatures there remain subsidiary loss mechanisms arising from the motion of side groups attached to the main chain. These latter motions have been identified not only in dynamic mechanical relaxation but also in dielectric relaxation,[1] NMR,[2-4] and neutron scattering.[5]

The barriers to rotation of methyl groups are relatively low compared to those of other side groups allowing a fairly fast rotational motion between sites, and the corresponding relaxation "peaks" are often difficult to observe in mechanical or NMR experiments because they occur as broad peaks at very low temperatures. The rather higher observation frequency of neutron scattering experiments together with the use of deuterium labeling has led to successful identification of methyl group libration within a potential well for a number of polymers via inelastic scattering,[6-9] and barrier heights to rotation have been calculated. Furthermore, the observation of rotational "hopping" over the barriers has been achieved via quasi-elastic scattering.[5,8]

The predominant effect on the rotational barriers of methyl side groups has been shown to be the chemical structure of the monomer unit, but in a few cases the stereoregularity produces a variation of 50% or more.[7] In the case of poly(methyl methacrylate) (PMMA) (Figure 1) the barrier height to rotation for the α-methyl group has been evaluated from inelastic neutron scattering (assuming that the observed frequency mainly corresponds to the 1–0 torsional transition within a threefold symmetric potential, V_3) and shown to vary from 23 kJ mol^{-1} for the isotactic form to 32 kJ mol^{-1} for the syndiotactic form.[7] Furthermore, activation energies as determined by NMR[4] vary from 15.5 to 22.6 kJ mol^{-1} for the two stereoisomers, respectively. If this increase is due to the nonbonded interactions between the α-methyl and the ester groups which are nearest neighbors in the syndiotactic PMMA (conformations of the two stereoisomeric forms of PMMA are shown in Figure 1), then a similar effect of stereoregularity might be expected also for the ester methyl group motions.

The torsional motion of the ester methyl group is observed in the inelastic neutron scattering spectrum to occur at a lower frequency than that for the α-methyl group,[6,7] indicating a lower barrier to rotation. The rotational hopping motion over this low barrier is correspondingly fast, allowing the motion to be well resolved in quasi-elastic neutron scattering experiments at low temperatures where all the other molecular motion has been frozen out. A measure of the barrier height may then be inferred from

0024-9297/84/2217-0560$01.50/0